Journal of Applied Fluid Mechanics, Vol. 12, No. 3, pp. 845-855, 2019.
Available online at www.jafmonline.net, ISSN 1735-3645, EISSN 1735-3645.
DOI: 10.29252/jafm.12.03.29531

Effective Boundary Conditions and Numerical Method for Flow Characteristics of Aeroengine Compressor at High Mach Flight

A. Q. Lin[1], J. Zhou[2, 3], X. J. Tian[3], Q. Zheng[1] and H. Zhang[1†]

[1] *College of Power and Energy Engineering, Harbin Engineering University, Harbin, 150001, Heilongjiang Province, China*
[2] *Science and Technology on Altitude Simulation Laboratory, jiangyou 621703, Sichuan Province, China*
[3] *AECC Sichuan Gas Turbine Establishment, jiangyou 621703, Sichuan Province, China*

†*Corresponding Author Email: zhanghai83821@163.com*

(Received August 14, 2018; accepted September 18, 2018)

ABSTRACT

Flow characteristics inside the compressor are of great importance for aeroengine performance under the high adverse pressure gradient. To meet the need for quick performance estimation, the numerical simulation is a meaningful investigation method to predict the similarity flow characteristics of aeroengine compressor at high Mach flight. Thus, this paper aims to satisfy the accuracy of compressor flow field at high altitude based on the similarity criterion. The accuracy for solution results by the application of the similarity criterion and the derivation of compressor boundary conditions is verified with the experimental data. Then, the parametric definitions of air intake are put forward to get the inlet boundary conditions of compressor. The comparative simulation results are conducted between similarity and prototype flow fields at design boundary conditions. The results show that among the most important dimensionless criterion is Mach number at high-speed flow, so the same equivalent mass flow and equivalent speed are recommended. In addition, the flow characteristics of the compressor at high altitude and high Mach number have a good similarity. Consequently, it can extend to further study compressor performance of aeroengine at different flight altitudes and Mach numbers.

Keywords: Aeroengine compressor; High Mach; Similarity criterion; Parametric definition.

NOMENCLATURE

a	acoustic velocity	p_R	total pressure ratio of compressor
C	dimensionless scaling coefficient	p_T	total pressure at any point of flow field
c_f	free stream velocity		
C_p	specific heat of air	PF	prototype flow field
ΔCp	coefficient of total pressure	R_g	gas constant
ΔCv	coefficient of velocity	Re	Reynolds number
1-D	one-dimensional	SF	similarity flow field
3-D	three-dimensional	T	static temperature
Eu	Euler number	T^*	total temperature
Fr	Froude number	T_R	total temperature ratio of compressor
G	mass flow	u	velocity
$\bar{G}$	equivalent mas flow	v	velocity at any point of the flow field
H	flight altitude	x, y, z	Cartesian coordinate
ISA	International Standard Atmospheric	η	efficiency of compressor
L	characteristic length	κ	specific heat ratio
Ma	Mach number		
n	rotational speed	λ	thermal conductivity
$\bar{n}$	equivalent rotational speed	μ	dynamic viscous
P	static pressure	ρ	air density
P^*	total pressure	σ	total pressure recovery coefficient

1. INTRODUCTION

Compressor is an important component of aero-engine, which is to compress the air by high-speed rotation blade and then to increase the pressure energy of the air, so as to improve the economy of the engine and increase the thrust of the engine. However, the flow loss inside the compressor is of great importance for aero-engine performance under the high adverse pressure gradient, especially for the tip leakage flow (Kuang *et al.*, 2017) and secondary flows such as passage vortex, trailing edge shedding vortex and radial fluid migration to blade boundary layer (Li *et al.*, 2014, Ramzi *et al.*, 2013). Besides, the shock wave transitional boundary layer interactions formed easily under the transonic or supersonic conditions results in a larger surface heat transfer than laminar or turbulent interactions (Hadjadj *et al.*, 2015, Sharma *et al.*, 2018). It is valuable to investigate the flow characteristics of compressor effectively.

However, the performance change for aero-engine is much more complex with respect to the improvement of flight range and speed. Among the common methods for investigating the internal flow of aeroengine compressor at high altitude and high Mach number flights are mainly experimental technology, the scaling model and numerical simulation. In many situations, experiments with a real object are usually difficult or even impossible to conduct due to measurement complexity or long-running test cycle. However, the scaling research is one of the most effective means to realize what the overall performance could be predicted from the scale models. In addition, the scale models based on the similarity criterion have been accepted and widely applied in many studies. For instance, a scale rocket engine model which is used in experimental research of the flow characteristics in combustion (Wang *et al.*, 2010) and a scale gas flow field model based on physical properties (Zhang *et al.*, 2016). The dimensionless similarity criteria include Reynolds number, Froude number, Euler number and Mach number, etc. However, it is impossible to satisfy the whole of the similarity criteria (Gao, 2002). Saha *et al.* (2011) experimentally investigated similarity criteria of Reynolds number and jet momentum ratio applied in the gas emission of two scale models. They found that, for most of the dimensionless parameters, only partial similarity between the model and the prototype can be satisfied. Therefore, the similarity to flow field may be not necessary for all parameters to guarantee the same, especially there is a conflict between the similarity requirements. For example, the Mach number could be neglected for low-speed or high-speed flows without regard to the compressibility effect (Gromke *et al.*, 2008); the Reynolds number could be ignored when it surpasses a specified value (Schwartzentruber *et al.*, 2007). Simultaneously, the numerical method is also widely applied in simulating such flows by applications of Reynolds-averaged Navier-Stokes (Lin *et al.*, 2018), Large Eddy Simulation (Shadloo *et al.*, 2018) and Direct Numerical Simulation (Shadloo *et al.* 2017). Thus, to further validate the accuracy of the similarity criterion by a Computational Fluid Dynamics method, the boundary conditions would be given by the requirement of similarity criteria, so that the calculation results are in good agreement with the criteria applied (Tang *et al.*, 2014).

The previous work shows the application of similarity criterion is a promising and efficient method to achieve the scaling flow field. In present study, therefore, new ideas are provided for the analysis of the scaling flow field of aero-engine compressor under a flight of high altitude and high speed. The NASA Stage 35 is used as a computation model which is applied to verify the accuracy of the flow field between the prototype and similarity flow fields. This method can capture the flow characteristics in details with flight state in high altitude, and the further investigation on the performance of compressor can be conducted such as precooling treatment for the higher inflow temperature.

2. SIMILARITY AND MODELING METHOD OF COMPRESSOR

In the condition of high altitude and high-speed flow, the total pressure loss will be gradually produced larger with air flowing through the air intake, which is a process of reducing the flow velocity and rising the flow temperature. Thus, the inflow conditions for total temperature and total pressure occur also change in the front of the compressor as shown in Fig. 1. For simulation on the performance of engine compressor at higher speeds and altitudes, the model of air intake and compressor should be established by similarity and modeling theory (*i.e.*, redefining some performance parameters of the compressor). From this, one-dimensional (1-D) modeling parameters of air intake can be derived into three-dimensional (3-D) inlet boundary conditions of compressor to further simulate the performance of compressor under high altitude flight.

This study takes compressor of NASA Stage 35 as a research object. The design performance parameters of Stage 35 (*i.e.*, the prototype) are obtained in the sea level standard atmospheric state. To acquire detailed parameters of Stage 35 with design point at a high altitude and high speed (*i.e.*, the scaling model), the compressor should be met the similarity criterion playing a role with its significance. The following explores the similarity theory to acquire the requirement of Stage 35 performance at a high altitude, and the flowchart is shown in Fig. 2.

2.1 Similarity Criterion for Compressor

The similarity criterion is the theoretical basis of compressor design and simulation experiment through analyzing the similarities between geometry structure and physical phenomena. Moreover, it should satisfy the requirement of three conditions: geometric similarity, flow field

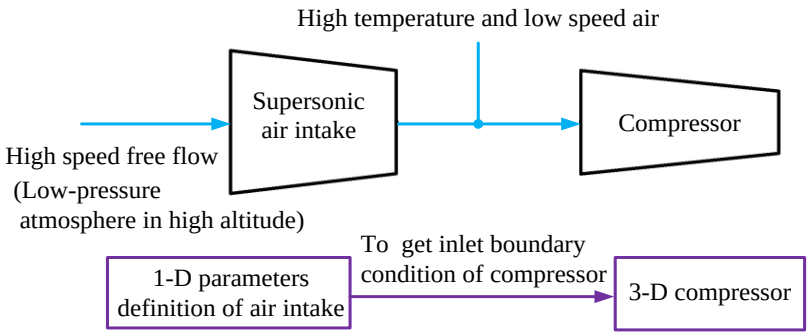

Fig. 1. Derivation process of compressor boundary conditions at high altitude flight.

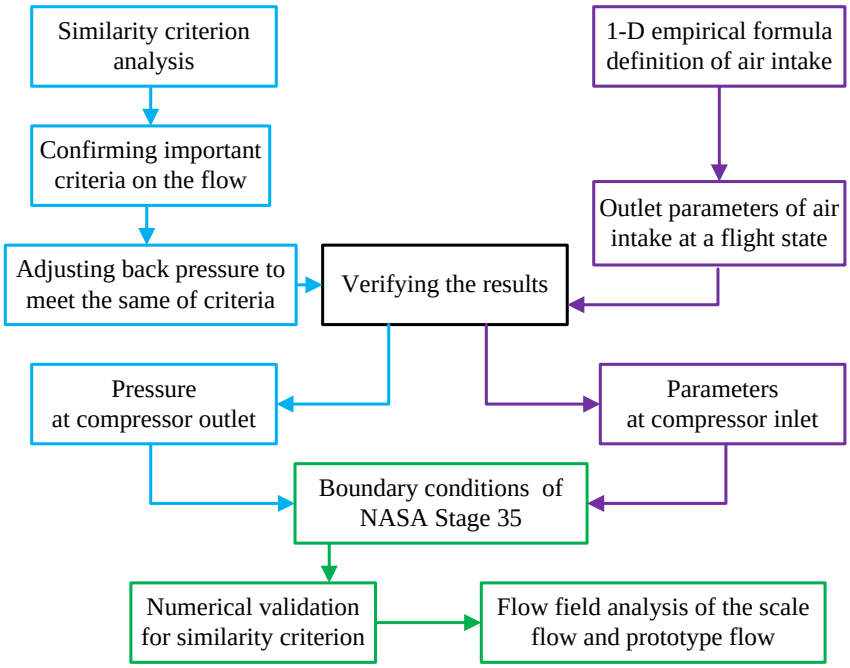

Fig. 2. Flowchart of research method and numerical simulation for the comparison between the scaling model and the prototype.

similarity (*i.e.*, kinematic similarity) and dynamic similarity. Here the hypothesis on geometries and fluid medium for two flow fields are kept unchanged. Hence, the kinematic and dynamic similarity can be verified by comparing the accuracy of the internal flow before and after applying the similarity and modeling methods for Stage-35 compressor. According to the Navier-Stokes equations, the motion differential equation of unit volume of fluid for compressible viscosity gas can be written as:

$$\partial(\rho\vec{u})/\partial t+\rho(\vec{u}\cdot\nabla)\vec{u}=\rho\vec{g}-\nabla p+\mu\nabla^2\vec{u}+\mu\nabla(\nabla\cdot\vec{u})/3 \tag{1}$$

For steady flow, $\partial(\rho\vec{u})/\partial t=0$, the motion differential equation can be changed into Eq. (2).

$$\rho(\vec{u}\cdot\nabla)\vec{u}=\rho\vec{g}-\nabla p+\mu\nabla^2\vec{u}+\mu\nabla(\nabla\cdot\vec{u})/3 \tag{2}$$

where, the term on the left side is the inertial force, the first and second terms on the right side are the gravity force and pressure, respectively, and then, the rest terms on the right side are the source term that is viscosity caused by the friction force.

Since the flow maintains similar, the motion equations of the Eq. (1) and Eq. (2) are proportional to each physical quantity at the corresponding geometric points as shown in Eq. (3).

$$\begin{cases} x_2/x_1=y_2/y_1=z_2/z_1=C_l, \\ u_2/u_1=C_u, \rho_2/\rho_1=C_\rho, g_2/g_1=C_g, \\ p_2/p_1=C_p, \mu_1/\mu_2=C_\mu. \end{cases} \tag{3}$$

where, C_l, C_u, C_ρ, C_g, C_p, C_μ are the dimensionless scaling coefficients of the relevant physical quantities. The subscript 1 of variables is the prototype flow field, and the subscript 2 is the scaling flow field. Then, the differential equation of motion (*i.e.*, Eq. (4)) can be obtained by substituting the Eq. (3) into Eq. (2).

$$C_\rho C_u{}^2 \rho(\vec{u}\cdot\nabla)\vec{u} / C_l = C_\rho C_g \rho\vec{g} - C_p / C_l \nabla p + C_\mu C_u \mu\nabla(\nabla\cdot\vec{u}) / 3C_l^2 \quad (4)$$

When the similarity criteria of the compressor are used for similarity transformation, the combinations of the scale coefficients in the basic equations are invariant, which can be given by:

$$C_\rho C_u^2 / C_l = C_\rho C_g = C_p / C_l = C_\mu C_u / C_l^2 \quad (5)$$

Deformation of the Eq. (5) can be simplified as:

$$C_l C_g / C_u{}^2 = C_p / C_\rho C_u{}^2 = C_\rho C_l C_u / C_\mu = 1 \quad (6)$$

Therefore, the relation between physical quantities at corresponding geometric points are obtained by similarity transformation of motion equations, which can be expressed by the formula below:

$$\frac{g_1 l_1}{u_1{}^2} = \frac{g_2 l_2}{u_2{}^2}, \ \frac{p_1}{\rho_1 u_1{}^2} = \frac{p_2}{\rho_2 u_2{}^2}, \ \frac{\rho_1 u_1 l_1}{\mu_1} = \frac{\rho_2 u_2 l_2}{\mu_2} \quad (7)$$

The dynamic similarity of flow field mainly depends on the dimensionless criteria of Reynolds number, Froude number, Euler number and Mach number, which should be all equal to a constant. Then, the Reynolds number (*Re*) is given by Eq. (8).

$$Re = \rho u L / \mu = \text{Const} \quad (8)$$

The physical meaning of *Re* is the ratio of the inertial force to the viscous force, which reflects the influence of fluid viscous on flow. When *Re* is large enough (*i.e.*, exceeding a particular value of *Re*≥2e+05), the air flows into the automatic modeled area, and the viscous force is very weak relative to the inertial force so that the whole flow process is no longer affected. Assuming that the inlet radius of the aero-engine is *L*=0.5 m and the intake speed is *u*=200 m/s, the Reynolds numbers at different flight altitudes (*H*) are listed in Table 1 according to the data from the International Standard Atmospheric (ISA).

Table 1 Reynolds number at different flight altitudes

H	ρ	$\mu\times10^5$	*Re*
/(km)	/(kg/m^3)	/(N·s/m^2)	/
0	1.225	1.789	6 846 149
5	0.736	1.628	4 521 343
10	0.413	1.457	2 832 338
15	0.194	1.422	1 362 338
20	0.088	1.422	619 231
25	0.039	1.449	272 325

As depicted in Table 1, in most cases, the flow field can satisfy the requirement of $Re\geq2\times10^5$. Thus, the decisive effect of *Re* on the flow state can be neglected.

The dimensionless criterion of Froude number (*Fr*) is written as:

$$Fr = gl / u^2 = \text{Const} \quad (9)$$

where, *Fr* is the ratio of gravity to inertia force. Since the air is forced to flow in the compressor, the influence of gravity on the flow can be negligible relative to other forces. Accordingly, the *Fr* can be considered unchanged.

The dimensionless criterion of Euler number (*Eu*) is given as:

$$Eu = p / \rho u^2 = \text{Const} \quad (10)$$

where, *Eu* is the ratio of pressure to inertia force. When the air velocity is very high, the acoustic velocity of $a = \sqrt{\kappa p / \rho}$ is usual substituted into Eq. (10) to derive the following equation:

$$\kappa u^2 / a^2 = \text{Const} \quad (11)$$

where, the physical meaning of Eq. (11) is the ratio of inertia force to the compressive force which reflects the influence of gas compressibility on flow.

The dimensionless criterion of Mach number (*Ma*) is calculated from Eq. (12).

$$Ma = u / a \quad (12)$$

Since the flow medium before and after modelling compressor is the air and the specific heat ratio of κ is the same in the similar flow process, the Eq. (12) can be expressed as Eq. (13) below.

$$u / a = \text{Const} = Ma \quad (13)$$

Therefore, in the case of geometric similarity, Mach number of compressor inlet should be kept similarity for high-speed flow. In the actual flow process, the radial velocity is much smaller than both the axial velocity (u_a) and the circumferential velocity ($u_c = 2\pi Ln / 60$ where n is the revolution speed, r/min), so the flow in the compressor is major axial and circumferential flow. In order to ensure that flow fields before and after modelling method are similar to the velocity triangle along each radial cross-section, both the axial Mach number of $Ma_a = u_a / \sqrt{\kappa RT}$ representing the velocity level and the circumferential Mach number of $Ma_c = u_c / \sqrt{\kappa RT}$ representing the flow magnitude should be guaranteed equal.

The following Eq. (14) can be acquired according to the condition where Mach numbers are equal in the circumference and axial directions.

$$u_{PF} / \sqrt{\kappa RT_{PF}} = u_{SF} / \sqrt{\kappa RT_{SF}} \quad (14)$$

where the subscript *PF* is the prototype flow field, the subscript *SF* is the similarity flow field. For the same physical properties of the flow medium, Eq. (14) can be simplified as:

$$n_{PF} / \sqrt{T_{PF}} = n_{SF} / \sqrt{T_{SF}} \quad (15)$$

Also, the similarities between axial Mach and velocity triangle of the compressor are given below:

$$u_{a(PF)} / u_{c(PF)} = u_{a(SF)} / u_{c(SF)} \tag{16}$$

$$V = u_c \pi L^2 \tag{17}$$

$$G = \rho VA = PVA / RT \tag{18}$$

Hence, Eq. (19) representing the flow field before and after modeling methods is derived according to Eqs. (16)-(18).

$$G_{PF} \sqrt{T_{PF}} / P_{PF} = G_{SF} \sqrt{T_{SF}} / P_{SF} \tag{19}$$

The Eq. (15) and Eq. (19) are the equivalent rotational speed and equivalent mass flow, respectively. To facilitate a practical application, it is necessary to translate the static temperature (T_{PF} and T_{SF}) and the static pressure (P_{PF} and P_{SF}) into the total temperature (T^*_{PF} and T^*_{SF}) and the total pressure (P^*_{PF} and P^*_{SF}), respectively, for Eq. (20) and Eq. (21).

$$T^*_{PF} / T_{PF} = T^*_{SF} / T_{SF} \tag{20}$$

$$P^*_{PF} / P_{PF} = P^*_{SF} / P_{SF} \tag{21}$$

In consequence, for simulating flow field of the compressor at ground operation to adapt a high-altitude flight surrounding, the equivalent mass flow ($\bar{G}$) and the equivalent rotational speed ($\bar{n}$) for compressor should be kept the same. The modeling method can be guaranteed which two flow fields are approximately similar. The similarity criterion can be determined by the following formula:

$$\left(\bar{G},\ \bar{n}\right) = \left(G\sqrt{T^*} / P^*, n / \sqrt{T^*}\right) \tag{22}$$

2.2 Parameters Definition of Air Intake

The passage from engine inlet to compressor inlet is called as the air intake. In flight, the flight Mach number is larger than the inlet Mach number of the compressor since the air intake can reduce airflow velocity and enlarge airflow pressure to fulfill normal operation of the compressor. One of the key parts of this study is the given boundary conditions of the compressor based on the known upper atmospheric parameters. Furthermore, to obtain more accurate inflow parameters of the compressor at high altitude and high Mach number flight, the analysis of intake process and the method of 1-D empirical formula definition are carried out as the following research, as shown in Fig. 3.

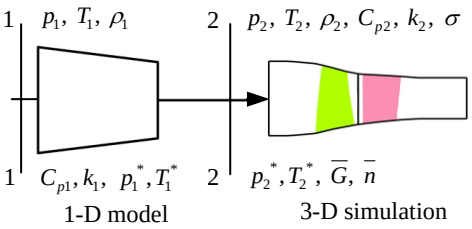

Fig. 3. Derivation process of 1-D empirical formulation in the air intake.

The local acoustic velocity and free stream velocity are calculated from Eq. (23) and Eq. (24), respectively, according to the known ISA data of local temperature, pressure, and density in a flight altitude.

$$a = \sqrt{\kappa R_g T} \tag{23}$$

$$c_f = a \times Ma \tag{24}$$

Considering the effect of high temperature, the specific heat of air varies with temperature. So, the five coefficients are used to fit the specific heat C_p of air (Poling *et al.*, 2001) as shown in Eq. (25).

$$C_p / R_g = b_0 + b_1 T + b_2 T^2 + b_3 T^3 + b_4 T^4 \tag{25}$$

where, the five coefficients are of b_0 = 3.653, b_1 = -1.337×10^{-3}, b_2 = 3.294×10^{-6}, b_3 = -1.913×10^{-9}, b_4 = 0.2763×10^{-12}, R_g is the gas constant.

Since the gas constant, R_g=287.15 J/(Kg·K), is related to different species of gas and is irrespective of the state of gas, the constant pressure specific heat at the inlet of the air intake can be obtained by Eq. (25), and the specific heat ratio of air is calculated from Eq. (26).

$$\kappa = C_p / (C_p - R_g) \tag{26}$$

After knowing the flight Mach number and atmospheric parameters, the total pressure and total temperature of the free stream can be received from Eq. (27) and Eq. (28), respectively.

$$P^* = P[1 + (\kappa - 1)Ma^2 / 2]^{\kappa/(\kappa-1)} \tag{27}$$

$$T^* = T[1 + (\kappa - 1)Ma^2 / 2] \tag{28}$$

In this study, it is assumed that the Mach number decreases to subsonic when the air flows through the outlet of the air intake, meanwhile the air flowing into the air intake is an adiabatic process. The following expressions are given by:

$$C_{P_1} T_1^* = C_{P_2} T_2^* \tag{29}$$

$$P = \rho R_g T \tag{30}$$

$$P_1^* = \sigma P_0^* \tag{31}$$

In the light of the MIL-E-5007D specification proposed in the 1970s U.S. released "General Specification of Aviation Turbojet and Turbofan" the estimation formulas of total pressure recovery coefficient of air intake under different flight Mach number are introduced in details. To accurately estimate the flow loss along air intake, the total pressure recovery coefficient of the air intake (σ) is used, as shown in Eq. (32).

$$\begin{cases} \sigma = 1, & 0 \le Ma \le 1 \\ \sigma = 1 - 0.075(Ma - 1)^{1.35}, & 1 \le Ma \le 5 \\ \sigma = 800/(935 + Ma^4). & Ma \ge 5 \end{cases} \tag{32}$$

where, Ma is the flying Mach number in the front of

air intake.

From the definition of the 1-D model for the air intake and ISA data, the outlet parameters of the air intake can be gained at different flight trajectories, as shown in Table 2. The outlet parameters of the air intake are considered as the inlet parameters of compressor. Among of 10 km from to 30 km flight paths, the outlet parameter at 26.82 km altitude is calculated by the Lagrange interpolation function.

The accuracy of the defined parameters for the air intake is verified with experimental data for the compressor inlet parameters at flight altitude of 26.82 km and flight Mach number of Ma=3.5 (Preston *et al.*, 2002). The comparative results between formula defined and data from the literature are shown in Table 3.

Table 2 Outlet parameters of the air intake under different flight trajectory

H	Ma	σ	T_2^*	P_2^*
/km	/	/	/K	/Pa
10	1.5	0.97	323.79	94 202.6
15	2.5	0.87	482.29	179 104.7
20	3	0.81	590.82	162 640.5
25	3.3	0.77	675.74	110 467.2
26.82	3.5	0.74	754.8	113 198.3
30	4	0.67	877.43	119 023.8

Table 3 Comparison of compressor inlet parameters between formula derived and data in literature

Data	T_2^*/K	Error	P_2^*/Pa	Error
Formula derived	754.8	0.03%	113198	0.18%
Data in literature	755		113400	

From Table 3, it can be understood that, by comparing different total temperature and total pressure at the compressor inlet, the relative errors of total pressure and total temperature are 0.178% and 0.026%, respectively. On the whole, comparing the experiment data, the compressor inlet parameters from empirical formula defined by 1-D air intake model show a higher accuracy on predicting outlet parameters of the air intake (*i.e.*, inlet parameters of compressor).

3. NUMERICAL METHOD

3.1 Computation Mesh and Numerical Model

With the intention of verifying the feasibility between the prototype and similarity flow field at high altitudes, the numerical method is applied to simulate flow field of Stage-35 which is according to the requirements of typical aircraft engine design of transonic compressor (Reid and Moore, 1978; Moore *et al.*, 1980). The Stage-35 has 36 rotor blades with tip clearance of 0.408 mm and 46 stator blades, as shown in Fig. 4. The boundaries at the circumferential direction are simplified as the rotational periodicity interfaces, and the interface between rotor outlet and stator inlet applies the mixing plane method. Then, all other walls are set to adiabatic and non-slip velocity boundary condition. Thus, the simplified geometry model with its mesh is shown in Fig. 5.

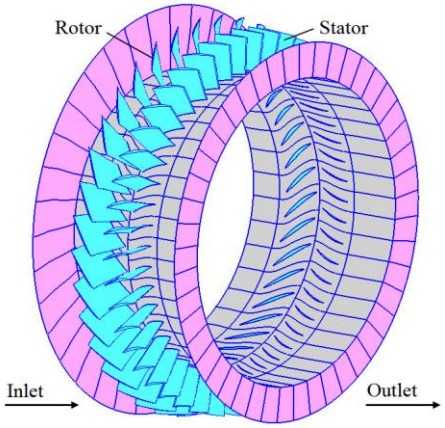

Fig. 4. Schematic diagram of NASA Stage-35 for an advanced high-pressure-ratio core compressor.

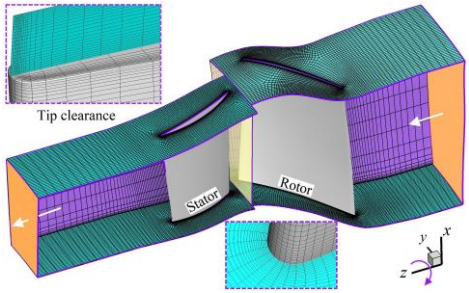

Fig. 5. Simplified geometry model and three-dimensional structured grid and details of tip clearance and blade edge grids in Stage-35.

Table 4 Performance parameters at experiment design point of stage-35 compressor

Design parameters	Values	Design parameters	Values
Rotative speed (r/min)	17188.7	Total temperature ratio	1.22
Mass flow (kg/s)	20.188	Total pressure ratio	1.82
Inlet total temperature (K)	288.15	Efficiency (%)	82.8

The design parameters of Stage-35 at the ground test are shown in Table 4. The present simulation uses commercial code Fluent 17.0 to solve the governing equations of 3-D compressible Reynolds-averaged Navier-Stokes, which is conducted on a parallel computer. The convergence criteria of Second-order Upwind accuracy for steady

computations are based on less than the levels of the order of 1×10^{-6}, and less than 0.1% mass flow error between inlet and outlet of Stage 35.

For high temperature air, dynamic viscosity (μ) and thermal conductivity (λ) are taken from Sutherland's law (Lin *et al.*, 2019). So, the physical property for C_p, μ and λ as the temperature changes is shown in Fig. 6.

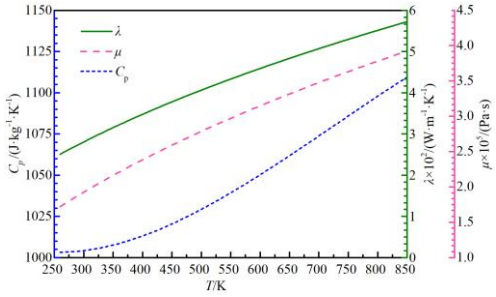

Fig. 6. Properties of dry air only varying with temperature.

3.2 Boundary Conditions and Turbulence Model

The boundary conditions are given according to experimental data of Stage-35. For 26.82 km altitude and *Ma*=3.5, total pressure and total temperature are assigned to the inlet boundary with detailed data seeing formula derived in Table 3. Moreover, the outlet boundary is subjected to static pressure (*i.e.*, back pressure) by which outlet pressure is gradually adjusted from 110 kPa to 170 kPa to capture the same equivalent mass flow with the prototype, so as to get the characteristic lines of the compressor. Then, a comparison of the characteristic lines between the numerical solution results (*i.e.*, the similarity) and experimental data including design point (*i.e.*, the prototype data) are shown in Fig. 7. The results demonstrate that, under the same equivalent mass flow of 3.38×10^{-3}, total pressure ratio is higher for simulation point than for experiment design point, while the efficiency is smaller for experiment point than for experiment design point. However, total pressure ratio of simulation point exceeds design point but is below experiment point; the efficiency of simulation point is larger than that of design point but is less than that of experiment point. As depicted in the figure, it is evident that characteristics of total pressure ratio and efficiency of simulation point are between experimental point and design point, and the shape of characteristics for simulation point and experimental point is approximately the same. Furthermore, the mathematical model established in this study agrees well with experimental data. When back pressure for simulation results reaches 159.590 kPa, the equivalent mass flow of similarity flow filed is the same as that of the prototype where this back pressure is static pressure of compressor outlet at design point of *H*=26.82 km and *Ma*=3.5.

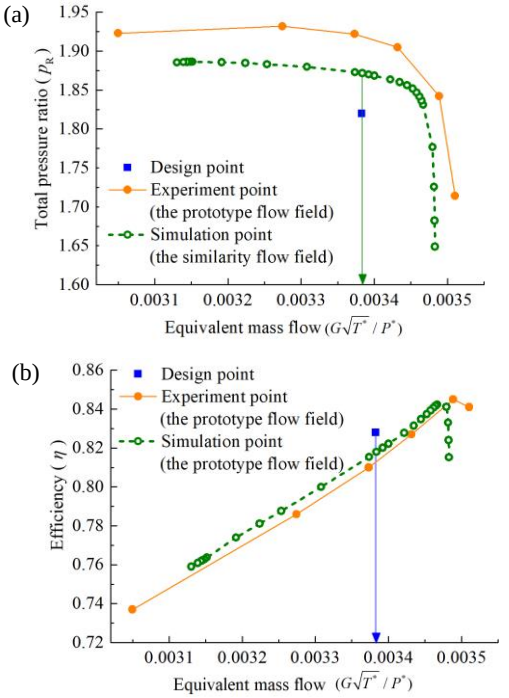

Fig. 7. A comparative solution results between experiment data (*i.e.*, prototype flow field) and high-altitude conditions of *H*=26.82 km and *Ma*=3.5 (*i.e.*, similarity flow field) for (a): total pressure ratio and (b): efficiency characteristics.

For the ground test conditions (*i.e.*, the prototype flow field), the numerical procedure validation of calculation accuracy is conducted by comparison with NASA experimental data (Reid and Moore, 1978), as shown in Fig. 8. For low-Reynolds and high-Reynolds number turbulence model, these computation grids are different with low y^+ and high y^+ values, respectively. Fig. 8 compares the error on total temperature ratio, T_R, total pressure ratio, p_R, and efficiency, η, relative to experimental results with the six CFD turbulence model predictions. The results predicted by the high-Reynolds number κ-ε and RNG κ-ε models possess a larger error and noticeable upstream shift for p_R and η. For low-Reynolds number turbulence models, however, there is no significant effect on the solutions, and the predicted results agree well with the experimental data. Based on the comparison of different models above, the SST κ-ω model is optimal in regard to simulation accuracy on predicting the flow characteristics of Stage-35 compressor. Simultaneously, after total grid cells above 1.50 million, the solution result is very little affected by the computational grid. Thus, the SST κ-ω turbulence model and 3.27 million grid cells with low y^+ value are considered in the prototype flow field. Moreover, the wall boundary layer distributes at least sixteen mesh cell nodes to meet the requirement of calculation solution inside the viscous sub-layer.

As depicted in Fig. 7, the equivalent mass flow is

3.38×10^{-3} due to a given boundary condition of aeroengine compressor. For the similarity flow field at high altitude and high Mach, Fig. 9 gives the solution results (*i.e.*, normalized total pressure ratio and normalized efficiency) at different turbulence models to compare with the degree of deviation of equivalent mass flow. As shown in the figure, different turbulence models have different effects on the solution results. The degree of deviation of equivalent mass flow is higher for high-Reynolds number κ-ε and RNG κ-ε turbulence models than for low-Reynolds number SST κ-ω and κ-ω Gamma turbulence models. In addition, the equivalent mass flow for the SST κ-ω turbulence model is consistent with $\bar{G}$ = 3.38×10^{-3}. On the whole, it can be substantiated that, for the prototype and similarity flow fields, the SST κ-ω turbulence model shows a higher accuracy on the prediction of flow characteristics of compressor.

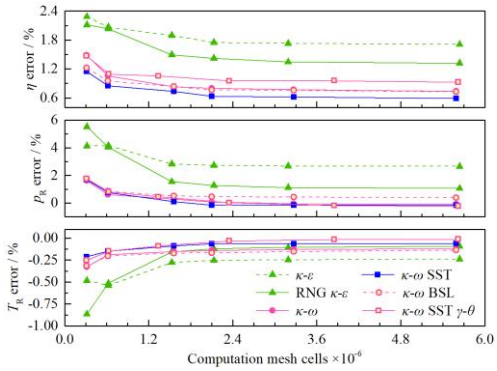

Fig. 8. Sensitivity investigations of computation mesh and turbulence model by comparing with the relative errors between numerical results and experimental data.

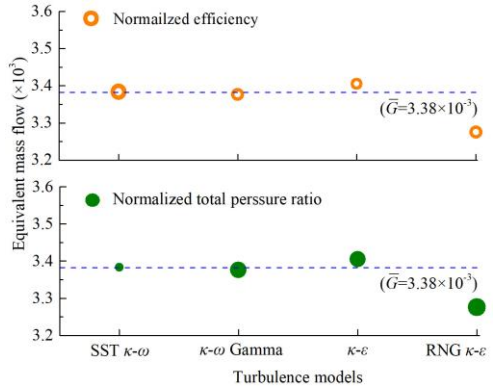

Fig. 9. A comparative deviation of the equivalent mass flow at different turbulence models under the similarity flow field.

4. RESULTS AND DISCUSSION

4.1 Analysis of Flow Field Similarity

In order to verify the accuracy and feasibility of numerical simulation by the application of the similarity criterion at the condition of H=26.82 km and Ma=3.5 (*i.e.*, the similarity flow field at design point), the comparative solution results are conducted with the experimental design point (*i.e.*, the prototype at design point). As illustrated in Figs. 10 and 11, the dimensionless contours of total pressure and velocity are analyzed at the rotor outlet. The dimensionless parameters of total pressure (ΔCp) and velocity (ΔCv) are presented in Eq. (33) and Eq. (34), respectively.

$$\Delta C\mathrm{p}=p_{\mathrm{T}} / p_{\mathrm{T,max}} \tag{33}$$

$$\Delta C\mathrm{v}=v / v_{\mathrm{max}} \tag{34}$$

where p_{T} and v are total pressure (Pa) and velocity (m/s) at any point of the flow field, respectively, $p_{\mathrm{T,max}}$ and v_{max} are the local maximum of total pressure and velocity, respectively.

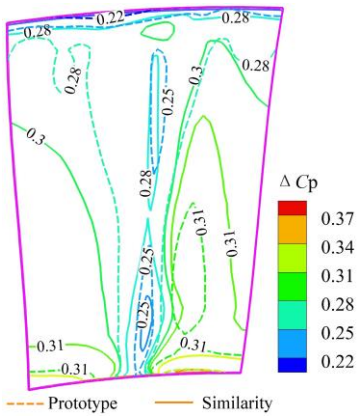

(a)

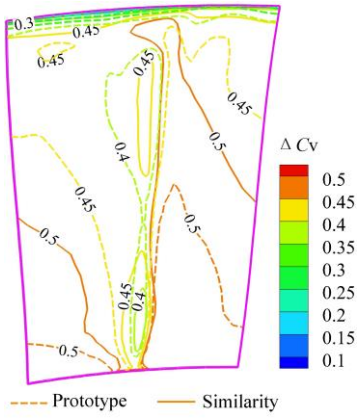

(b)

Fig. 10. Flow characteristics of (a): total pressure and (b): velocity between prototype and similarity flow fields at rotor outlet.

As shown in Fig. 10, two flow fields have approximately the same lower value zones of total pressure and velocity at the meridional of rotor outlet and closing to the shroud, which effects on the wake flow of blade trailing edge. Although the value distributions for ΔCp and ΔCv are some different, the dimensionless value regions are the same. It can be ascribed primally that the flow structures are changed from the ground level test to igh altitude conditions.

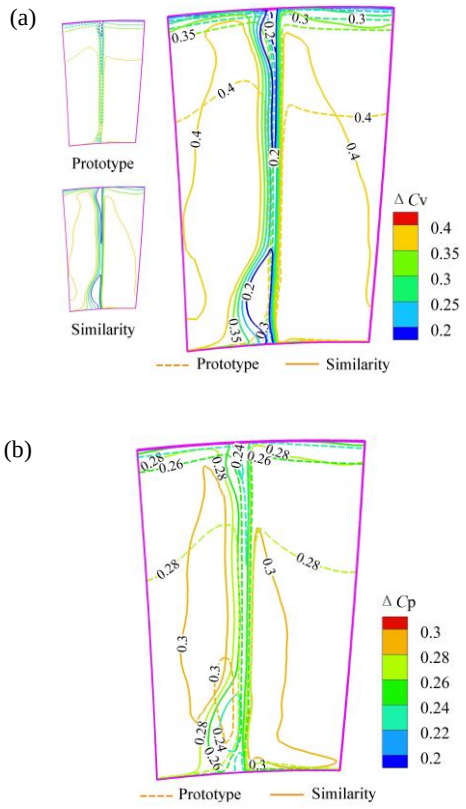

Fig. 11. Flow characteristics of (a): total pressure and (b): velocity between prototype and similarity flow fields at stator outlet.

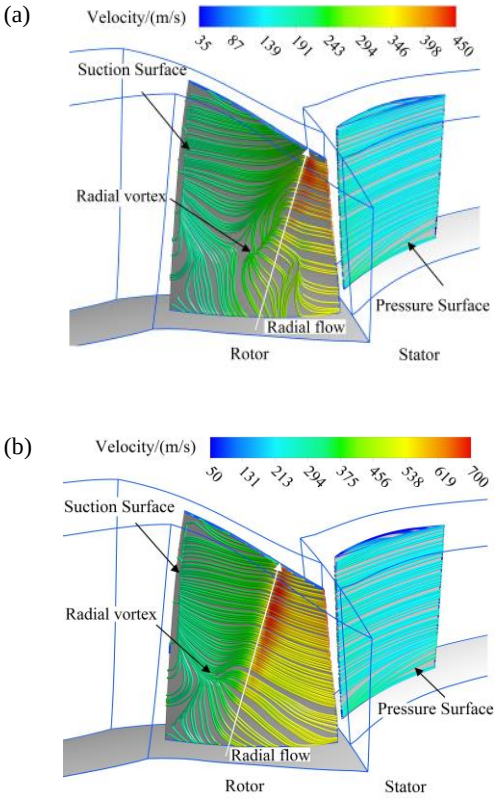

Fig. 12. Limiting streamline structures near the blade walls of Stage 35 for (a): prototype and (b): similarity flow fields.

As can be seen in Fig. 11, the lower value zone at the meridional plane of stator outlet, influenced by the wake flow at the trailing edge, is divided into two major higher value zones for total pressure and velocity. Moreover, the flow field distributions of two conditions possess similar to a certain extent.

Thus, form Figs. 10-11, it can be concluded that, for pressure and velocity, the flow characteristics of two flow fields are similar by the analysis of dimensionless method. Then, this phenomenon illustrates that those flow parameters of the motion equations corresponding geometric points for similarity flow field are proportional to that for the prototype flow field.

In Fig. 12, it is obvious that the limiting streamlines closing to blade surface have some similar flow characteristics, such as existing the corner separation at the suction surface, the radial secondary flow, and wall flow separation. And the radial flow along blade height direction and closing to the trailing edge of rotor blade constantly rolls the air flow at the suction surface. Simultaneously, the air flow smoothly passes through the pressure surface of stator blade without producing any separation flow for two flow fields. As a result, the flow field similarity in the compressor exists the motion equations proportional to the physical quantities before and after modeling.

4.2 Analysis of Dynamic Similarity

The contours of inlet Mach number under the absolute frame are given in Fig. 13. It is clearly shown that inlet Mach number gradually increases along blade height and basically keeps consistent at the cross sections of each elementary level between the prototype and similarity flow fields.

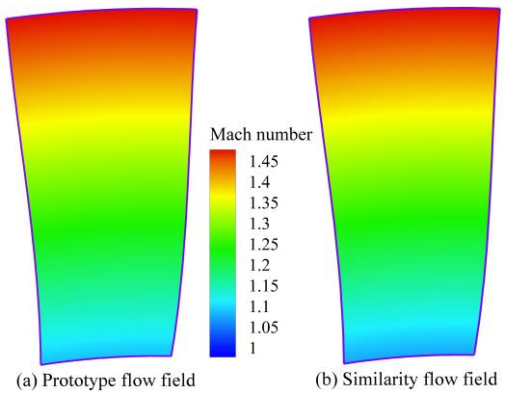

Fig. 13. Mach contours of the (a): prototype and (b): similarity flow fields on the compressor inlet.

To analyze the similarity of the velocity triangles on the rotor outlet, the Mach number contours are shown in Fig. 14. Since the effect of high-speed rotation, there exists a slight difference for Mach number distribution closing to the hub and shroud. However, the majority of Mach number in the mainstream region remain similar, which can be further substantiated that the velocity triangle of similarity flow field is in close to that of the prototype flow field.

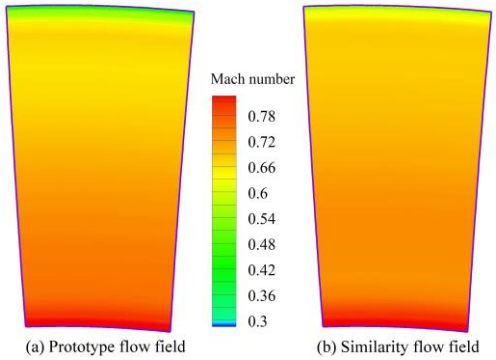

Fig. 14. Mach contours of the (a): prototype and (b): similarity flow fields on the stator inlet.

To summarize, the results show that the flow fields in Stage 35 compressor before and after applying the similarity criterion can meet the dynamic similarity. In view of the formula derivation above for similarity criterion (*i.e.*, the flow field modeling process), the similarity modeling and the boundary conditions derivation methods are appropriate to predict the flow characteristics and aerodynamic performance in the aeroengine compressor at high altitude and high Mach flight conditions.

5. CONCLUSION

A numerical method is conducted for the flow characteristic prediction in an aeroengine compressor with the focus to investigate the effective boundary conditions of compressor at high altitude and high Mach flight. The calculation accuracy for results was qualified by comparing with the experimental data. Results show that, an effective method getting the inlet boundary conditions of the compressor is to derive the 1-D model parametric definitions of the air intake. At high altitude and high Mach, the dimensionless criterion of Mach number is the most significant influence on the flow characteristic in the case of geometric similarity, so the equivalent mass flow and equivalent rotational speed are recommended to maintain the same at the compressor inlet. By comparison with the prototype and similarity flow fields, the flow characteristics of compressor at high altitude condition have a good similarity comparing with the NASA experimental design point. Besides, the performance of compressor at high altitude has a higher accuracy by using the similarity criterion. It is therefore that this study would enable to further investigate the flow characteristics and aerodynamic performance of aeroengine compressor at different flight altitudes and Mach numbers.

ACKNOWLEDGEMENTS

The authors would like to thank the support of the National Natural Science Foundation of China Nos. 51409067 and 51809065, and the Fundamental Research Funds for the Central Universities (Nos. HEUCF180305 and HEUCFJ180301). In addition, Aqiang Lin especially wishes to thank the understanding and support from his elder brother Zhicai Lin.

REFERENCES

Gao, Y. W. (2002). *Experimental Fluid Dynamics*. China Northwestern Polytechnical University Press, Xian, China.

Gromke, C. and B. Ruck (2008). Aerodynamic modelling of trees for small-scale wind tunnel studies. *Forestry* 81(3), 243-258.

Hadjadj, A., O. Ben Nasr, M. S. Shadloo and A. Chaudhuri (2015). Effect of wall temperature in supersonic turbulent boundary layers: A numerical study. *International Journal of Heat and Mass Transfer* 81, 426-438.

Kuang, H., S. W. Chu, H. Zhang and S. Ma (2017). Flow mechanism for stall margin improvement via axial slot casing treatment on a transonic axial compressor. *Journal of Applied Fluid Mechanics* 10(2), 703-712.

Li, X. J., W. L. Chu and H. G. Zhang (2014). Investigation on relation between secondary flow and loss on a high loaded axial-flow compressor cascade. *Journal of Propulsion Technology* 7, 914-925.

Lin, A. Q., Q. Zheng, L. Yang and H. Zhang (2019). Effect of inlet air pre-cooling of water injection on compressor performance at high flight mach. *Journal of Applied Fluid Mechanics* 12(2), 421–431.

Lin, A. Q., Y. G. Sun, H. Zhang, X. Lin, L. Yang and Q. Zheng (2018). Fluctuating characteristics of air-mist mixture flow with conjugate wall-film motion in a compressor of gas turbine. *Applied Thermal Engineering* 142, 779-792.

Moore, R. D. and L. Reid (1980). *Performance of single-stage axial-flow transonic compressor with rotor and stator aspect ratios of 1.19 and 1.26 respectively, and with design pressure ratio of 2.05*, NASA, TP-1659.

Poling, B. E. and J. M. Prausnitz (2001). *The properties of gases and liquids*. McGraw-Hill, New York, USA.

Preston, H. C. and V. Balepin (2002). Mass injection and pre-compressor cooling engines analyses. *AIAA* 2002-4127.

Ramzi, M. and G. Abderrahmane (2013). Passive Control via Slotted Blading in a Compressor Cascade at Stall Condition. *Journal of Applied Fluid Mechanics* 6(4), 571–580.

Reid, L. and R. D. Moore (1978). *Design and overall performance of four highly-loaded, high-speed inlet stages for an advanced, high-pressure-ratio core compressor*, NASA, TP-1337.

Saha, C. K., G. Q. Zhang, J. Q. Ni and Z. Y. Ye (2011). Similarity criteria for estimating gas emission from scale models. *Biosystems*

Engineering 108(3), 227-236.

Schwartzentruber, T. E., L. C. Scalabrin and I. D. Boyd (2007). A modular particle-continuum numerical method for hypersonic non-equilibrium gas flows. *Journal of Computational Physics* 225(1), 1159-1174.

Shadloo, M. S. and A. Hadjadj (2017). Laminar-turbulent transition in supersonic boundary layers with surface heat transfer: A numerical study. *Numerical Heat Transfer Part A - Applications* 72(1), 40-53.

Shadloo, M. S. and A. Hadjadj (2017). Laminar-turbulent transition in supersonic boundary layers with surface heat transfer: A numerical study. Numerical Heat Transfer Part A - Applications 72(1), 40-53.

Shadloo, M. S., A. Hadjadj, A. Chaudhuri and O. Ben-Nasra (2018). Large-eddy simulation of a spatially-evolving supersonic turbulent boundary layer at M_∞=2. *European Journal of Mechanics - B/Fluids* 67, 185-197.

Sharma, S., M. S. Shadloo and A. Hadjadj (2018). Laminar to turbulent transition in supersonic boundary layer: Effects of initial perturbation and wall heat-transfer. *Numerical Heat Transfer, Part A: Applications* 73, 583-603.

Tang, Z., B. He and G. Cai (2014). Investigation on a coupled navier-stokes-direct simulation monte carlo method for the simulation of plume flowfield of a conical nozzle. *International Journal for Numerical Methods in Fluids* 76(2), 95-108.

Wang, X. W., G. B. Cai and P. Jin (2010). Scaling of the flowfield in a combustion chamber with a gas-gas injector. *Chinese Physics B* 19(1), 019401.

Zhang, M. X., G. B. Cai, B. J. He and Z. Y. Tang (2016). Investigation of similarity criterion for gas flow field based on physical properties. *European Journal of Mechanics - B/Fluids* 60, 196-208.